



Cite this: *J. Mater. Chem. C*, 2020, **8**, 98

# Theoretical perspective for luminescent mechanism of thermally activated delayed fluorescence emitter with excited-state intramolecular proton transfer†

Guanyu Jiang, Feiyan Li, Jianzhong Fan,  Yuzhi Song, Chuan-Kui Wang\* and Lili Lin  \*

Excited-state intramolecular proton transfer (ESIPT) and thermally activated delayed fluorescence (TADF) are interesting photochemical and photophysical properties for light-emitting materials. Recently, a novel design strategy for TADF molecules was realized in the TQB molecule by ESIPT [*ACS Cent. Sci.*, 2017, **3**(7), 769–777]; however, the TADF and ESIPT mechanisms for this molecule are not very clear. In this work, the TADF and ESIPT mechanisms for TQB in both solution and the solid phase were studied based on the calculation of potential energy curves, energy levels and decay rates of the excited states. It was found that proton transfer in  $S_1$  for TQB is quite easy in both DMF and the solid phase. In contrast, the proton transfer in  $T_1$  and  $T_2$  in DMF is slightly difficult, while the barrier in  $T_1$  for TQB in the solid phase is comparable with room temperature energy. The  $^1T_2\text{TQB-TA} \rightarrow ^1S_1\text{TQB-TB}$  upconversion path plays a crucial role in the TADF of TQB in solvent, while  $^1T_2\text{TQB-TB} \rightarrow ^1S_1\text{TQB-TB}$  has a dominant contribution to the TADF in the solid phase. Based on the investigation of TQB, we designed two molecules, TQB\* with a single hydrogen bond and TQB\*\* with two hydrogen bonds. Our calculation results indicate that the TQB\*\* molecules can realize dual emission by ESIPT and are a potential light-emitting material for white light. No ESIPT can be realized in TQB\*, while large energy gaps are found between the higher excited states and lowest excited states. Our investigation provides new perspectives for the ESIPT and TADF mechanisms, which can help in understanding the light-emitting properties of TQB and provide some insights on the design of new functional luminescent molecules.

Received 27th September 2019,  
Accepted 12th November 2019

DOI: 10.1039/c9tc05299b

rsc.li/materials-c

## 1 Introduction

Recently, thermally activated delayed fluorescence (TADF) materials have attracted wide attention since 100% exciton usage efficiency can be obtained in organic light-emitting diodes with TADF emitters.<sup>1</sup> Although great progress has been achieved for TADF emitters, most of them are composed of donors (D) and acceptors (A) to achieve a smaller energy gap ( $\Delta E_{ST}$ ) between the first singlet excited state ( $S_1$ ) and the lowest triplet excited state ( $T_1$ ) by separating the highest occupied molecular orbital (HOMO) and the lowest unoccupied molecular orbital (LUMO).<sup>2,3</sup>

However, some limitations of TADF molecules have also been observed. Although a separated HOMO–LUMO is favorable for obtaining a small  $\Delta E_{ST}$ , it results in reduced radiative rates. To overcome these shortcomings, molecules designed based on the opposite resonant effect,<sup>4</sup> dual emitting core,<sup>5</sup> combined charge-transfer pathways<sup>6</sup> and intramolecular proton transfer (ESIPT) process<sup>7</sup> have been reported. The ESIPT process is a classic photoisomerization process, which is a very fast four-level cyclic proton-transfer reaction between an enol (E) and keto (K) ( $E \rightarrow E^* \rightarrow K^* \rightarrow K \rightarrow E$ ).<sup>8,9</sup> Due to the abnormally large Stokes shift between the emission from  $K^*$  and the absorption from E, self-absorption can be avoided.<sup>10</sup> Actually, the first ESIPT molecule combined with the TADF phenomenon was first reported by Park *et al.* in 2007.<sup>11</sup> Nevertheless, this phenomenon is constrained to in solution only. In organic light-emitting diodes (OLEDs), the ESIPT process may be inhibited due to the environment confinement. The triquinolonobenzene (TQB) molecule reported by Mamada *et al.* is the first rigid TADF–ESIPT molecule without D or A groups, which can overcome the environmental limitation and realize TADF and ESIPT

Shandong Key Laboratory of Medical Physics and Image Processing & Shandong Provincial Engineering and Technical Center of Light Manipulations, School of Physics and Electronics, Shandong Normal University, Jinan 250358, China.  
E-mail: ckwang@sdsu.edu.cn, linll@sdsu.edu.cn

† Electronic supplementary information (ESI) available: The independent gradient model (IGM) method, the visualization of hydrogen bonds, the geometric parameters for  $S_1$ , the electron–hole distribution of all tautomers in  $T_1$  and  $T_2$ , and excitation energy and transition dipole moment of the designed molecules. See DOI: 10.1039/c9tc05299b

in OLEDs. Their work presented a new design strategy for TADF emitters. Nevertheless, the mechanisms of TADF and ESIPT are still very clear, although some theoretical works have focused on them. Cao *et al.* performed quantum chemistry and *ab initio* molecular dynamics calculations and found that the proton transfer from the triplet state of normal TQB to the singlet excited state of ESIPT TQB ( $^3\text{TQB-TA} \rightarrow ^1\text{TQB-TB}$ ) plays a crucial rule in triplet exciton harvesting.<sup>12</sup> Zhao *et al.* studied the influence of solution polarity on the ESIPT process and found that the ESIPT can be facilitated by polar solvents.<sup>13</sup> Why does the conversion from  $^3\text{TQB-TA}$  to  $^1\text{TQB-TB}$  play a crucial role in the triplet exciton harvesting of TQB? Are there any other pathways? What about the mechanism in the solid phase? Are the ESIPT process and RISC process similar to that in solvent? Herein, the TADF and ESIPT mechanisms were systematically studied in both solution and solid phase using the polarized continuum model (PCM) and the combined quantum mechanics and molecular mechanics (QM/MM) method. The excited-state decay rates were also calculated based on the thermal vibration correlation function (TVCF) method. In addition, two new molecules were designed based on TQB by breaking its symmetry and also studied for potential application as functional molecules.<sup>14</sup> Our theoretical results will not only be helpful for understanding the photophysical phenomenon of TADF-ESIPT molecules but also help in the design of new molecules.

## 2 Computational details and theoretical methods

In our research, the density functional theory (DFT) was used to optimize the molecular structure in the ground state ( $S_0$ ), while the geometry of the excited states was optimized with the time-dependent density functional theory (TD-DFT). All the above calculations were calculated at the B3LYP/6-31g(d) level. The PCM method was used in the calculation to simulate the solution environment and *N,N*-dimethylformamide (DMF) solvent was adopted. The reason why we chose to study the light-emitting properties of TQB in DMF is to compare the experimental results where measurements were performed in DMF, tetrahydrofuran (THF) and toluene. Since Cao *et al.* performed a theoretical simulation on the light-emitting mechanism of TQB in toluene,<sup>12</sup> we assumed it is better to study another solvent effect. Considering that DMF (with a permittivity constant of 37.2) is a much stronger polar solvent than toluene (with a permittivity constant of 2.4), the differences for TQB in toluene and in DMF may be more significant. In addition, ESIPT is sensitive to polar environments. If the polarity of the solution is too high, the ESIPT process will be difficult. However, TADF was found for TQB in DMF, which predicts that ESIPT should happen in DMF. Our calculation confirmed the results and it further proved that TQB is a good candidate for TADF emitters by the ESIPT process. For QM/MM calculation, a two-layer ONIOM model was adopted.<sup>15–18</sup> The central molecule was set as the high layer, and the QM method was used. The molecules around the central molecule were set as the low layer and calculated using the MM method with the efficient universal force field (UFF).

The MM part was frozen during the geometry optimizations for the all states in the QM/MM calculation. The potential energy curves along the proton transfer path for  $S_0$ ,  $S_1$  and  $T_1$  in DMF and the solid phase were also studied. All the abovementioned calculations were achieved in the Gaussian 16 package.<sup>19</sup>

Based on the abovementioned calculations, we calculated the decay rates of the excited states. The radiative rate of  $S_1$  was obtained using the Einstein spontaneous emission formula:

$$K_r = \frac{f \Delta E_{fi}^2}{1.499 \text{ cm}^{-2} \text{ s}} \quad (1)$$

where  $f$  is the oscillator strength and  $\Delta E_{fi}$  is the vertical emission energy with the unit wavenumber ( $\text{cm}^{-1}$ ).

According to Fermi's golden rule (FGR) and the first-order perturbation theory, the nonradiative decay rate can be written as follows:

$$K_{nr} = \frac{2}{\hbar^2} \sum_{\mu, \nu} P_{i\mu} |H_{f\mu, i\nu}|^2 \delta(E_{i\nu} - E_{f\mu}). \quad (2)$$

where  $P_{i\mu}$  is the Boltzmann distribution function of the initial state and  $H_{f\mu, i\nu}$  is the interaction between two different Born–Oppenheimer states, which it contains two contributions as follows:

$$\hat{H}\Psi_{i\nu} = \hat{H}^{\text{BO}}\Phi_i(r, Q)\Phi_\nu(Q) + \hat{H}^{\text{SO}}\Phi_i(r, Q)\Phi_\nu(Q). \quad (3)$$

where  $\hat{H}^{\text{BO}}$  denotes the nonadiabatic coupling and  $\hat{H}^{\text{SO}}$  is the spin–orbit coupling. When a Fourier transform is applied for the delta function, the intersystem crossing rate constant between two electronic states with different spin multiplicity can be written as:

$$K_{\text{ISC}} = \frac{1}{\hbar^2} \langle \Phi_f | \hat{H}^{\text{SO}} | \Phi_i \rangle \int_{-\infty}^{\infty} dt [e^{i\omega_{if}t} Z_i^{-1} \rho_{\text{ISC}}(t, T)] \quad (4)$$

where  $\rho_{\text{IC}}(t, T)$  is the thermal-vibration correlation function and  $Z_i$  is the partition function. Both the methodology and application of this formalism can be found in Peng and Shuai's reports.<sup>20–22</sup> The calculations mentioned above can be realized in the MOMAP (Molecular Materials Property Prediction Package promoted by the Institute of Chemistry Chinese Academy of Sciences and Department of Chemistry, Tsinghua University).<sup>23–25</sup>

## 3 Results and discussions

### 3.1 Geometrical structures

From the chemical structure of TQB, we can deduce that there should be three hydrogen bonds in TQB, and thus three proton transfer states may exist. The molecule without proton transfer is labeled as TQB-TA (shown in Fig. 1(a)). The molecule with one proton transferred is named TQB-TB (shown in Fig. 1(b)). The molecules with two and three protons transferred are called TQB-TC and TQB-TD (shown in Fig. 1(c) and (d)), respectively. To confirm the hydrogen bonds in TQB, the independent gradient model (IGM) method was used to investigate the inter-molecule weak interactions (shown in Fig. S1, ESI†).<sup>26</sup> Detailed information about this method can be seen in the Supplementary file. From Fig. S1 (ESI†), we can find obvious hydrogen bond interactions (HBI) at three parts for all the tautomers in both DMF and the

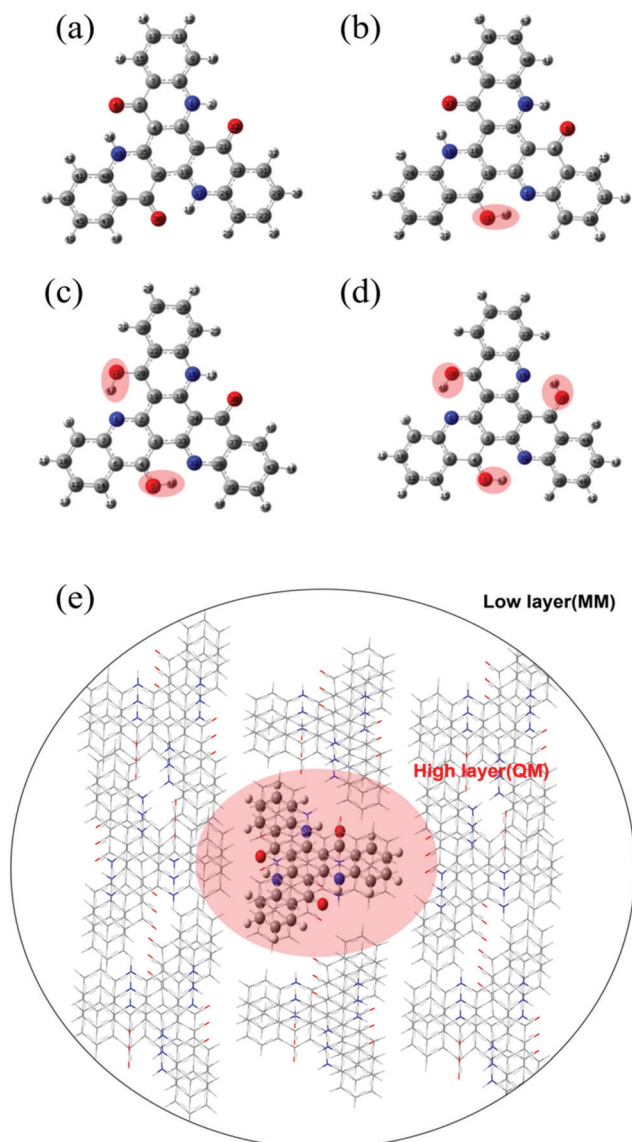


Fig. 1 Chemical structure of TQB-TA (a), TQB-TB (b), TQB-TC (c) and TQB-TD (d). The positions with proton transfer are marked in red. (e) ONIOM model: the centered TQB is treated as the high layer and surrounding molecules are regarded as the low layer.

solid phase. This means that proton transfer may occur at these three parts.<sup>27</sup> We tried to optimize the structure of all the tautomers to obtain the stable geometry. Unfortunately, the stable geometries of TQB-TB in  $S_0$  were not obtained in both DMF and the solid state, which is consistent with experimental result. Besides, the stable geometries of all the tautomers in the excited state were also optimized and only TQB-TD in  $S_1$  was not obtained. The results are consistent with the experimental result that TQB-TD is not detected experimentally. It should be noted that the optimization for TQB-TA in the solid state was performed based on the crystal structure of TQB obtained experimentally. For the optimization of TQB-TB, TQB-TC and TQB-TD in the solid phase, the crystal structure of TQB was also adopted with the central molecule TQB-TA changed to the molecule with a proton

Table 1 Emission wavelengths and oscillator strength calculated for all the tautomers in DMF and the solid phase

	DMF		Solid	
	$\lambda$ (nm)	$f$	$\lambda$ (nm)	$f$
TQB-TA	375	0.0000	374	0.0004
TQB-TB	513	0.2539	568	0.0909
TQB-TC	485	0.3694	576	0.0958
Exp.	542		520	

Exp. is experimental emission wavelength.

transferred. The QM/MM model is shown in Fig. 1(e). Since  $S_1$  is responsible for light emitting and proton transfer, some important geometric parameters for TQB-TA, TQB-TB and TQB-TC in  $S_1$  are listed in Table S1 (ESI<sup>†</sup>) for comparison (definitions of the parameters are shown in Fig. S2, ESI<sup>†</sup>). It can be found that the bond lengths and angles of the hydrogen bonds obviously change after the proton is transferred. There are no significant differences for the geometric structures except the dihedral angles in the solvent and solid phase. In the solid phase, the planarity of the hydrogen bond and also the symmetry of the molecule are destroyed.

To explore the light-emitting properties, the emission wavelengths of the three tautomers were calculated in both DMF and the solid phase, as shown in Table 1. It was found that the emission wavelengths for TQB-TA in DMF (375 nm) and the solid phase (374 nm) have a large discrepancy with the experimental values (542 nm). Nevertheless, the emission wavelengths for TQB-TB (513 nm) and TQB-TC (485 nm) in DMF are close to the experimental values. In addition, the values in the solid phase (568 nm and 576 nm) are also close to the experimental values (520 nm). It was deduced that the emission of TQB should come from TQB-TB or TQB-TC. Besides, we found that the oscillator strength for TQB-TA is zero, which indicates that TQB-TA is not responsible for light emitting. It also indicates that it should be easy for a proton to transfer from TQB-TA to TQB-TB. Are both TQB-TB and TQB-TC responsible for the emission? Is it actually easy for a proton to transfer from TQB-TA to TQB-TB? Is it also easy for a proton to transfer from TQB-TB to TQB-TC?

### 3.2 Emission mechanism in DMF

To further explore the emission process, the potential energy curve (PEC) along the nitrogen–hydrogen distance for TQB in DMF is shown in Fig. 2. Since the molecular geometry of TQB-TA is symmetric, the three hydrogen bonds should be equivalent in DMF. Both the first and second proton transfer were chosen randomly. From the potential energy curve of  $S_0$ , it can be found that the energy of TQB-TA is the lowest. The energy barrier from TQB-TA to TQB-TB is as large as 0.41 eV, which means that it is difficult for a proton to transfer in the ground state for TQB. From the potential energy curve of  $S_1$ , it can be found that TQB-TB is the most stable. The energy barrier from TQB-TA to TQB-TB is only 0.03 eV, which means it is easy for a proton to transfer from TQB-TQ to TQB-TB in the first excited state. The energy barriers from TQB-TB to TQB-TC and back to TQB-TA are as large as 0.48 eV and 0.41 eV, which indicates that it is difficult

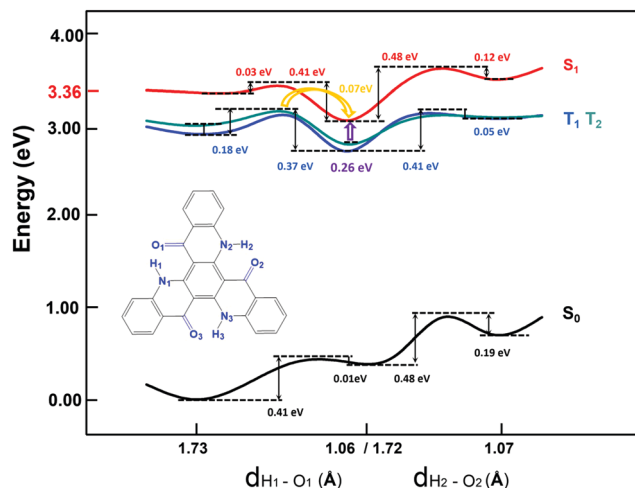


Fig. 2 Potential energy curves of TQB with ESIPT in DMF.

for double proton transfer and backward single proton transfer, respectively. The molecules tend to stay at TQB-TB in  $S_1$ , and thus the emission in DMF should come from TQB-TB not TQB-TC.

Besides, there TADF was also found for TQB. Thus, the TADF mechanism was also investigated. As is known, TADF is realized by upconversion from the triplet state to the first singlet excited state. Since TQB-TB is responsible for emission, upconversion may also occur in TQB-TB. The energy levels of several low-lying excited states for TQB-TB and other tautomers in DMF are

illustrated in Fig. 3. It can be found that there is one triplet excited state below  $S_1$  in energy for TQB-TB, and the energy gap between them is 0.26 eV. Although  $T_2$  is higher than  $S_1$  in energy, their energy gap is as small as 0.06 eV. Both  $T_1$  and  $T_2$  may participate in the reverse intersystem crossing (RISC) process, while the RISC efficiency should not be very high due to the relatively large energy gap between  $S_1$  and  $T_1$  as well as the low distribution of the molecule in  $T_2$ . To confirm our conclusions, the spin-orbit coupling (SOC) constants between  $S_1$  and  $T_1$  ( $T_2$ ) in DMF were calculated using the Dalton 2013 package (see Table 2).<sup>28</sup> It was found that the SOC constants for TQB-TA and TQB-TB are all quite small. The SOC values between  $S_1$  and  $T_2$  for TQB-TA are zero or close to zero. The SOC constants between  $S_1$  and  $T_1$  for TQB-TB are slightly larger than that between  $S_1$  and  $T_1$ . The ISC and RISC rates in DMF were also calculated, as shown in Table 3. For TQB-TB, the ISC and RISC rates between  $S_1$  and  $T_2$  are  $4.1 \times 10^4 \text{ s}^{-1}$  and  $1.5 \times 10^5 \text{ s}^{-1}$ , which shows contribution to the exciton decay. The ISC and RISC rates between  $S_1$  and  $T_1$  are only  $2.6 \times 10^2 \text{ s}^{-1}$  and zero, respectively, which may have little influence in the process of delayed fluorescence. Based on the analysis above, we think that one of the TADF conversion process in DMF is as follows:  $^3\text{TQB-TA} \rightarrow ^3\text{TQB-TB} \rightarrow ^3\text{TQB-TB} \rightarrow ^3\text{TQB-TB}$ .

Recently, Cao *et al.* proposed that the proton transfer along  $^3\text{TQB-TA} \rightarrow ^1\text{TQB-TB}$  plays crucial role in exciton harvesting. We also noticed that there are four triplet excited states lower in energy than  $S_1$  for TQB-TA. The energy gap between  $S_1$  and  $T_1$  is as large as 0.45 eV, and the gap between  $S_1$  and  $T_4$  is 0.22 eV.

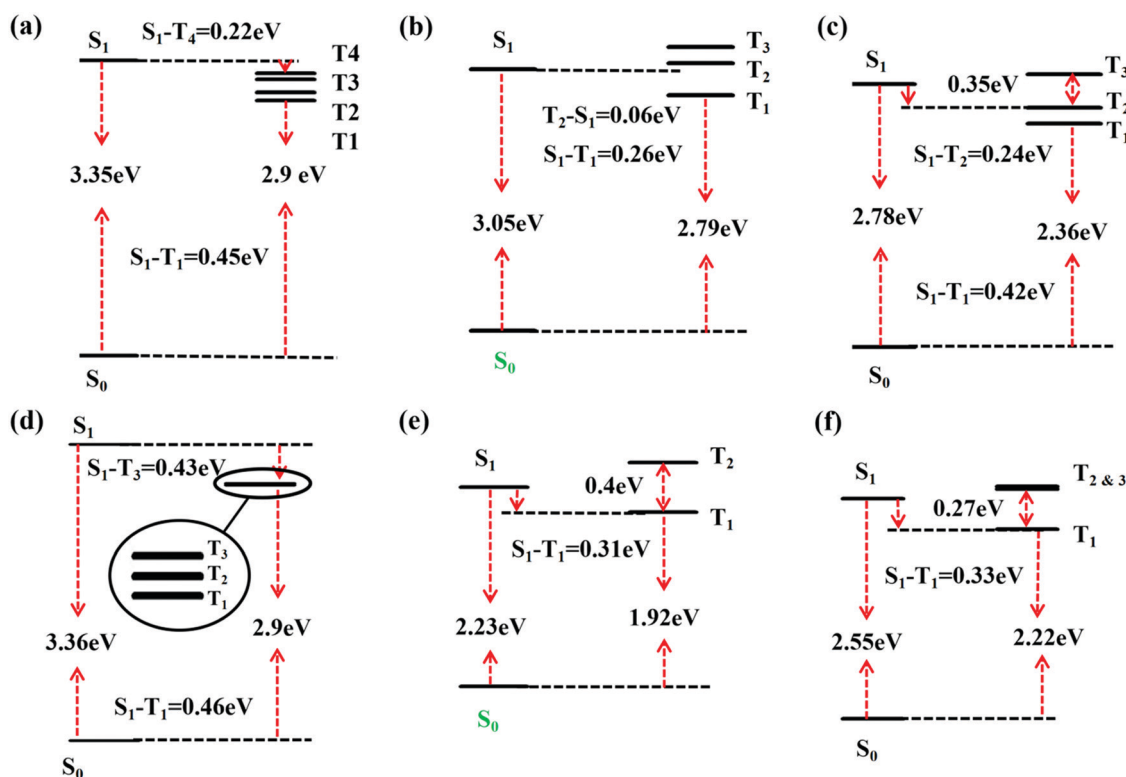


Fig. 3 Excitation energies based on the optimized geometry of every state for TQB-TA (a), TQB-TB (b), and TQB-TC (c) in DMF and TQB-TA (d), TQB-TB (e), and TQB-TC (f) in the solid phase.



**Table 2** Spin-orbit coupling (SOC) constants between  $S_1$  and triplet states

$H_{so}$ ( $\text{cm}^{-1}$ )	TQB-TA		TQB-TB	
	DMF	Solid	DMF	Solid
$S_1-T_1$	0.018	0.539	0.004	0.175
$S_1-T_2$	0.000	0.226	0.015	0.199
$T_1-S_1$	0.018	0.749	0.004	0.186
$T_2-S_1$	0.002	0.219	0.018	0.229

$S_1-T_n$  ( $n = 1$  and  $2$ ) based on the optimized single excited state structures and  $T_1-S_n$  ( $n = 1$  and  $2$ ) based on the optimized triplet excited states structures.

**Table 3** Correlation rate calculated for molecular TQB-TA, TQB-TB and TQB-TC in both DMF and the solid phase.  $K_r$  is the rate of radiative decay rate,  $K_{nr}$  is the nonradiative decay rate,  $K_{RISC}$  is the reverse intersystem crossing rate, and  $K_{ISC}$  is the intersystem crossing rate (unit:  $\text{s}^{-1}$ )

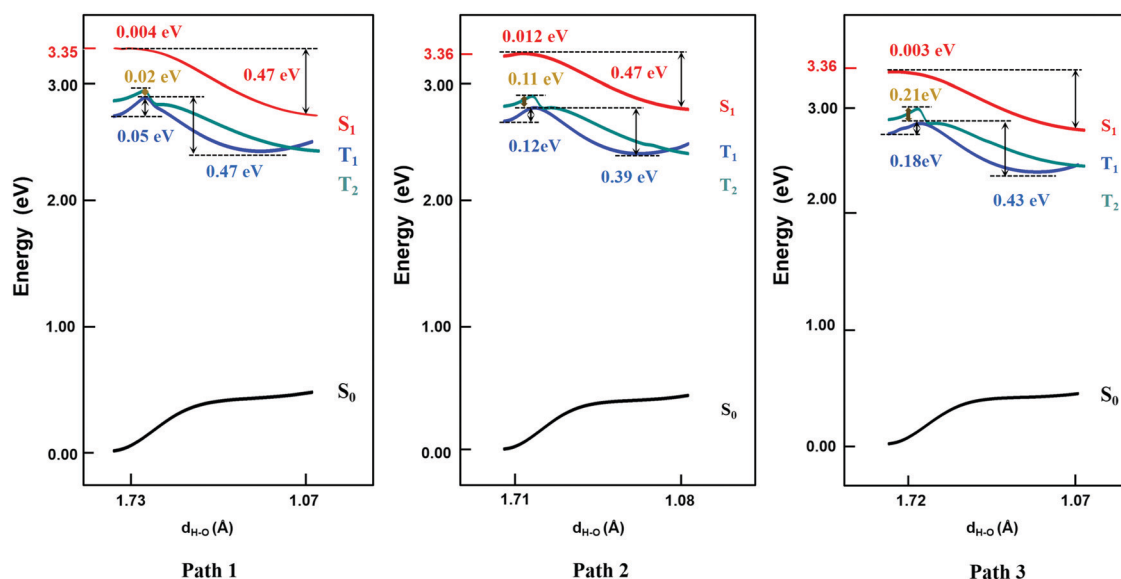
	TQB-TA		TQB-TB	
	DMF	Solid	DMF	Solid
$K_r (S_1 \rightarrow S_0)$	0	$1.6 \times 10^9$	$1.7 \times 10^8$	$1.9 \times 10^7$
$K_{ISC} (S_1 \rightarrow T_1)$	0	$3.8 \times 10^6$	$2.6 \times 10^2$	$8.3 \times 10^5$
$K_{ISC} (S_1 \rightarrow T_2)$	0	1.3	$4.1 \times 10^4$	$4.9 \times 10^6$
$K_{RISC} (T_1 \rightarrow S_1)$	0	2.1	0	6.18
$K_{RISC} (T_2 \rightarrow S_1)$	0	$1.1 \times 10^6$	$1.5 \times 10^5$	$7.9 \times 10^6$

Thus, it can be deduced that it is quite difficult to realize upconversion in TQB-TA. Since  $T_2$  in TQB-TA is lower than  $S_1$  and higher than  $S_1$  in TQB-TB, we deduce that there should be crossing between  $S_1$ -PEC and  $T_2$ -PEC. The potential energy curves of  $T_1$  and  $T_2$  were also studied (shown in Fig. 2). It was found that both  $T_1$  and  $T_2$  are stable in TQB-TB. However, we found that the energy barrier for  $T_1$  and  $T_2$  from TQB-TA to TQB-TB is 0.18 eV and 0.11 eV, respectively. This means that proton transfer is slightly difficult in the triplet excited states only relying on the thermal energy at room temperature. Nevertheless, we noticed that  $T_2$  of TQB-TA is close in energy to  $S_1$  in TQB-TB.

It is quite possible for a proton to transfer from  $T_2$  to  $S_1$ . This is also consistent with the conclusion by Cao *et al.*<sup>12</sup> Of course, it should be noted that most of the triplet states should be in  $T_1$  of TQB-TA. If the conversion from  $T_2$ TQB-TA  $\rightarrow$   $S_1$ TQB-TB is responsible for the exciton harvesting, the coupling between  $T_1$ TQB-TA and  $T_2$ TQB-TA should also be important. From the potential energy curve, we can find that the energy of  $T_1$  is really close to  $T_2$ , which could ensure coupling between them. This is also the reason why  $T_1$ TQB-TA is generated for photo excitation. Since the molecules are all first excited to the singlet states of TQB-TA for photoexcitation, the generation of  $T_1$ TQB-TA seems impossible by the ISC process since the ISC rate between  $T_1$ TQB-TA and  $S_1$ TQB-TA was calculated to be zero. However, the crossing between the surfaces of  $S_1$  and  $T_2$  as well as the coupling between  $T_1$  and  $T_2$  will favor its generation. Considering the difficulty in simulating the electroluminescent properties of molecules in the solid phase, the studies in solvent can also be seen as references for the electroluminescent properties in the solid phase.<sup>29</sup> For electroluminescence, more triplet excited states will be generated and the  $T_1$ TQB-TA  $\rightarrow$   $T_2$ TQB-TA  $\rightarrow$   $S_1$ TQB-TB process may play a more significant role. In the following section, we study the light-emitting properties of TQB in the solid phase, which can be used to analyze both its photo-luminescence and electro-luminescence properties.

### 3.3 Emission mechanism in the solid phase

Based on the results above, we found that it is easy for a proton to transfer from  $S_1$  of TQB-TA to TQB-TB in DMF. TQB-TB is responsible for light emitting. There are two TADF generation paths: (1)  $S_1$ TQB-TA  $\rightarrow$   $S_1$ TQB-TB  $\rightarrow$   $T_2$ TQB-TB  $\rightarrow$   $S_1$ TQB-TB and (2)  $T_1$ TQB-TA  $\rightarrow$   $T_2$ TQB-TA  $\rightarrow$   $S_1$ TQB-TB. What is the situation for TQB in the solid phase? Here, we also performed a relaxed scan of the potential energy curve of the molecule in the  $S_0$ ,  $S_1$  and  $T_1$  states (shown in Fig. 4). We found that the hydrogen bonds for TQB-TA in the solid phase are not equivalent due to

**Fig. 4** Potential energy curves of TQB with single proton transfer in the solid phase.

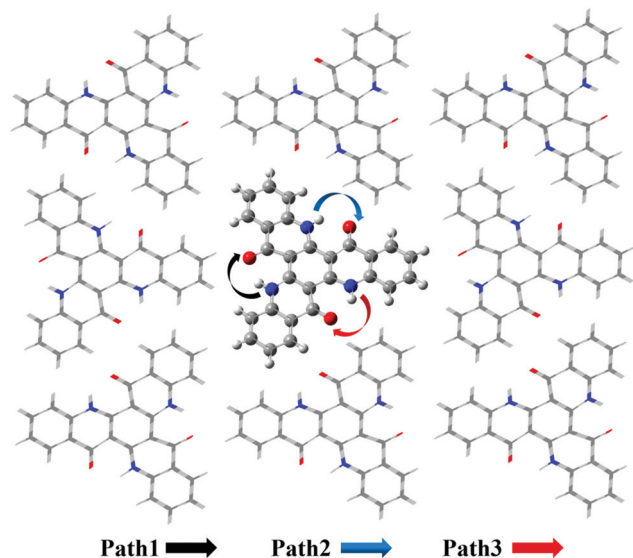


Fig. 5 Three proton transfer paths in the solid phase.

the different environments in the solid phase. For convenience, three paths are labeled, as shown in Fig. 5, and the single proton transfer process in the three paths was studied. It can be found that it is similar to the situation in DMF. The geometry of TQB-TA is more stable than that of TQB-TB in  $S_0$ , while TQB-TB is lower in energy than TQB-TA in  $S_1$ . The energy barriers from  $^5S_1$ TQB-TA to  $^5S_1$ TQB-TB are 0.004 eV, 0.012 eV and 0.003 eV for Path 1, Path 2 and Path 3, respectively. This means that all three paths are quite easy to be traversed although there is a slight difference among them. In comparison with the results in DMF, the proton transfer in  $S_1$  becomes almost barrier free in the solid phase. In addition, the energy barriers from  $^1T_1$ TQB-TA to  $^1T_1$ TQB-TB or from  $^3T_2$ TQB-TA to  $^3T_2$ TQB-TB in Path 1 are 0.02 eV and 0.05 eV, respectively, which is much smaller than that in Path 2 and Path 3. This means that proton transfer may also occur in triplet states along Path 1 in the solid phase, which is different from that in DMF. In the solid phase, both singlet and triplet excitons of TQB-TA can decay by proton transfer to TQB-TB.

Based on the above analysis, we deduce that TADF in the solid phase should also be realized in TQB-TB. To confirm this deduction, the energy levels of several low-lying excited states are illustrated in Fig. 3. It can be found that the energy gap between  $S_1$  and  $T_1$  in TQB-TB in the solid phase is 0.31 eV, while the gap between  $S_1$  and  $T_2$  is only 0.09 eV. This is similar to the situation in DMF, although the energy gaps are slightly larger. The energy gaps between  $S_1$  and  $T_1$  in TQB-TA and TQB-TC in the solid phase are still quite large. In addition, we calculated the SOC constants between  $S_1$  and  $T_1$  or  $T_2$  (shown in Table 2). It was found that the SOC constants for both TQB-TA and TQB-TB in the solid phase are much larger than that in DMF. The ISC and RISC rates in the solid phase were also calculated, as shown in Table 3. It is obvious that the ISC and RISC rates in the solid phase are also much larger than that in DMF. The ISC rates from  $S_1$  to  $T_1$  and  $T_2$  in TQB-TB are  $8.3 \times 10^5 \text{ s}^{-1}$  and  $4.9 \times 10^6 \text{ s}^{-1}$ , which means that both channels are responsible for

the ISC process. However, the RISC rate from  $T_1$  to  $S_1$  is very small, which means that the RISC process for TQB-TB should be from  $T_2$  to  $S_1$ . The TADF process in the solid phase is confirmed to be  $^3T_2$ TQB-TA  $\rightarrow$   $^3T_2$ TQB-TB  $\rightarrow$   $^5S_1$ TQB-TB and  $^1T_1$ TQB-TA  $\rightarrow$   $^1T_1$ TQB-TB  $\rightarrow$   $^3T_2$ TQB-TB  $\rightarrow$   $^5S_1$ TQB-TB. Of course, we cannot exclude the path  $^3T_2$ TQB-TA  $\rightarrow$   $^5S_1$ TQB-TB. From Fig. 3, it can be found that the energy of  $T_2$  in TQB-TA is lower than that of  $S_1$ , while it is higher than  $S_1$  in TQB-TB. From Fig. 4, it can also be found that the energy of  $T_2$  in TQB-TA is higher than that of  $S_1$  in TQB-TB, and thus energy crossing may also occur in the solid phase.

### 3.4 Oscillator strength and transition property of excited states

Based on the results above, we found that the oscillator strength for TQB-TA in DMF is zero, while it is much larger for TQB-TB (see Table 1). This means that the oscillator strength can be enlarged after proton transfer. The oscillator strength is highly related to the transition dipole moment (TDM) as follows:

$$f = \frac{2}{3} \Delta E |\langle i | -r | j \rangle|^2 \quad (5)$$

where  $f$  is the oscillator strength and  $\Delta E$  is the energy gap between two states,  $|i\rangle$  and  $|j\rangle$ .  $r$  is the displacement coordinate vector. Since the energy gap between  $S_1$  and  $S_0$  for TQB-TB is always smaller than that for TQB-TA, the enlarged oscillator strength should be induced by an increase in TDM. The visualization of TDM of the tautomers both in DMF and the solid phase is shown in Fig. 6. The TDM of TQB-TA is quite small, thus the oscillator strength of TQB-TA is close to zero both in DMF and the solid phase. The TDMs of TQB-TB and TQB-TC are clearly larger than that of TQB-TA. To determine why the TDM for TQB-TA is quite small, the molecule was divided into three parts according to symmetry. The TDM for every fragment in TQB-TA points to the center or departs from the center, and thus they counteract with each other. After proton transfer, the TDM of each fragment is different. The two fragments with proton transfer involved contribute to the TDM with a similar direction, and thus induce significant TDM for TQB-TB. In TQB-TC, the fragment with both sides including proton transfer shows little contribution to TDM, and the fragments with single side proton transfer contribute significantly to the TDM. This indicates that the TDM is correlated to the symmetry of the molecule.

In addition, the transition properties of the excited states were analyzed. Since more than one molecular orbital contributes to the excitation of  $S_1$ , the electron-hole distribution of the excited states for the three tautomers in DMF and the solid phase was analyzed (as shown in Fig. 7 and Fig. S3, S4, ESI†). From Fig. 7, it can be seen that the electrons and holes are distributed almost averagely in TQB-TA in both DMF and the solid phase. There is significant separation for electrons and holes in TQB-TB and TQB-TC. Electrons are mainly distributed on fragment 2 and holes are distributed on fragment 3 for TQB-TB, which mean that there is significant charge transfer from fragment 3 to fragment 2 during excitation. For TQB-TC, electrons and holes are located on fragments 1 and 3, respectively. The electron-hole distribution is also confirmed from the heat map shown in the figure,

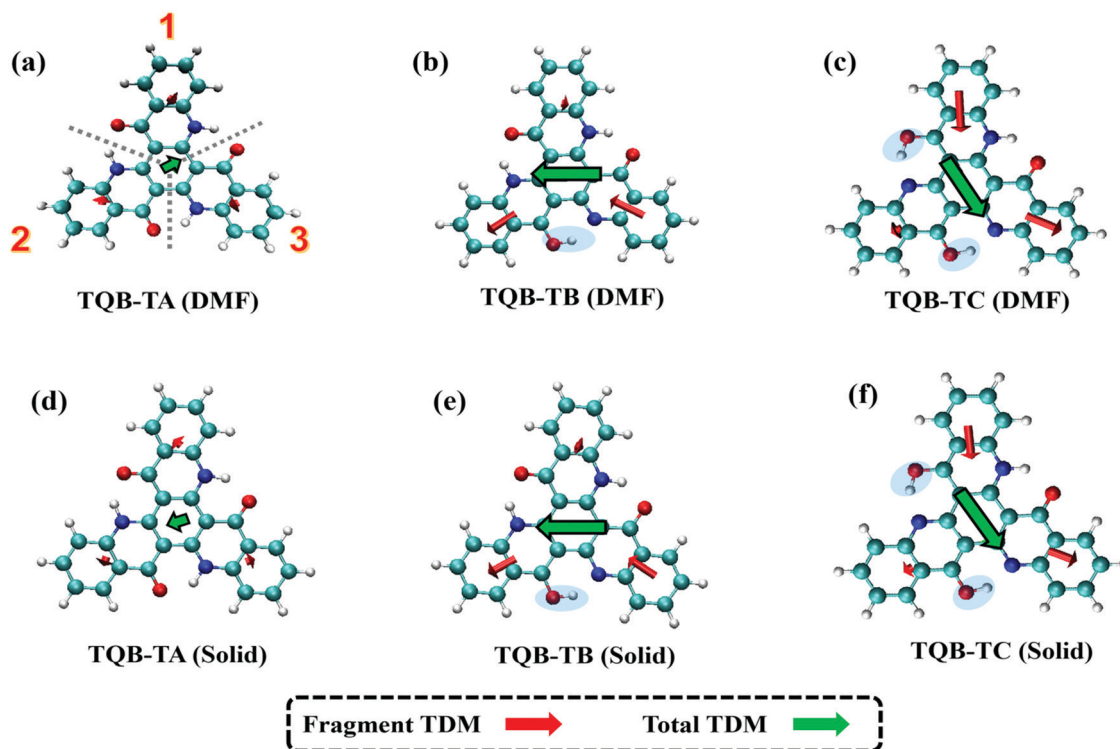


Fig. 6 Transition dipole moments (TDM) of TQB-TA, TQB-TB and TQB-TC in DMF (a–c) and the solid phase (d–f). For the analysis, the molecules were divided into three parts, as labeled in (a).

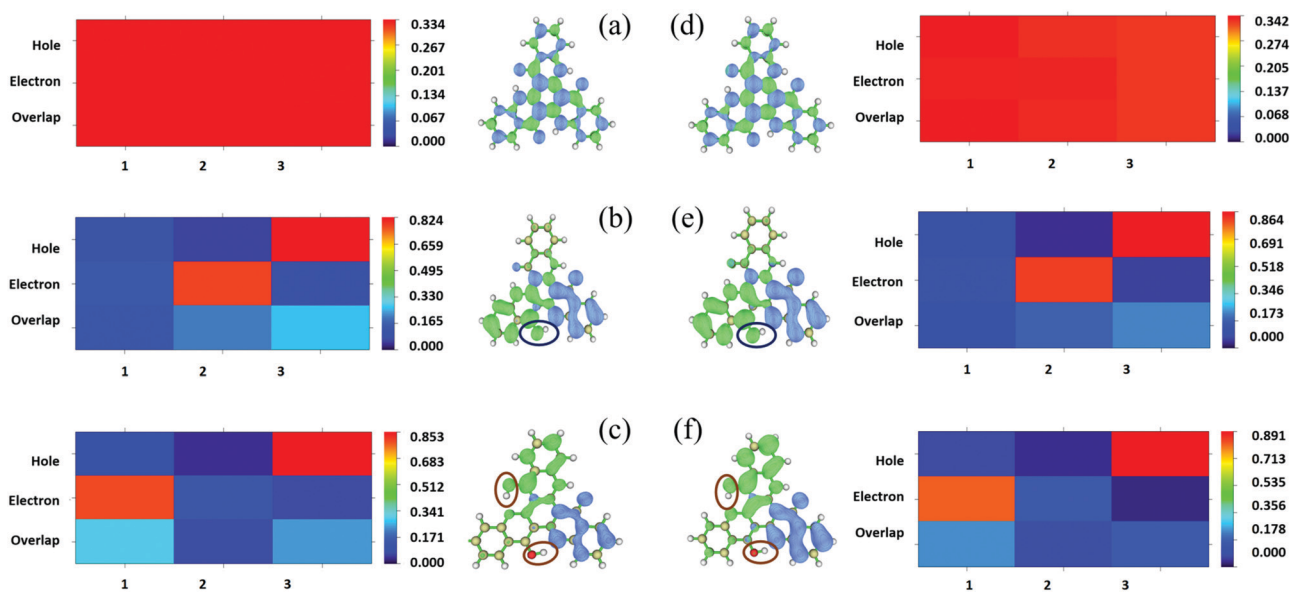


Fig. 7 Isosurface of the distribution for holes and electrons and heat map of TQB-TA (a), TQB-TB (b) and TQB-TC (c) in DMF and TQB-TA (d), TQB-TB (e) and TQB-TC (f) in the solid phase in the  $S_1$  state.

which was obtained using the Multiwfn package program.<sup>30</sup> Based on the electron–hole distribution, it can be concluded that the  $S_1$  state of TQB-TA is a typical locally excited (LE) state, and the  $S_1$  states for both TQB-TB and TQB-TC are charge-transfer states. Since  $S_1$ TQB-TB is generated from  $S_1$ TQB-TA by proton transfer, it can be concluded that the proton transfer

also induces electron transfer in the excited states. This also indicates that the direction of the proton transfer also influences the direction of the electron transfer. From  $S_1$ TQB-TA to  $S_1$ TQB-TB, a proton is transferred from fragment 3 to fragment 2, and thus electrons are transferred from fragment 3 to fragment 2. From  $S_1$ TQB-TB to  $S_1$ TQB-TC, one proton is transferred from fragment 3

to fragment 2, and the other proton is transferred from fragment 2 to fragment 1. It can be seen that the proton is transferred from fragment 3 to fragment 1 and no proton is gained or lost in fragment 2. Thus, we think that electrons are transferred from fragment 3 to fragment 1. It seems that proton transfer is also accompanied by electron transfer.

From Fig. S3 (ESI<sup>†</sup>), it can be found that TQB-TA is still an LE state in both DMF and the solid phase, although the LE is only localized on fragment 2 in the solid phase. Both TQB-TB and TQB-TC are still CT states in  $T_1$ , while there is also some LE component in the transition. For  $T_2$ , it can be seen that TQB-TA is still an LE state in both DMF and the solid phase, while the transition is only located on one fragment or two fragments (see Fig. S4, ESI<sup>†</sup>). For TQB-TB and TQB-TC, although CT is significant, more LE component is involved. The transition properties have a close relationship with the photophysical properties. Recent reports showed that vibration coupling between  $^3\text{CT}$  and  $^3\text{LE}$  states can provide new paths for upconversion.<sup>31–33</sup> The enhancement of the LE components in  $T_2$  of TQB-TB may favor the coupling between  $T_1$  and  $T_2$  and the upconversion process. In addition, the different natures of the singlet and triplet states can favor the ISC process by enhanced spin-orbit coupling.<sup>34</sup> The increase in LE component in  $T_1$  and  $T_2$  can also favor the ISC and RISC processes in TQB-TB. This is also consistent with our calculated SOC values, as shown in Table 2. In general, the LE transition is favorable for radiation since the oscillator strength is proportional to the overlap of excited states ( $f \propto -r|\langle i | j \rangle|^2$ ). Nevertheless, the oscillator strength of TQB-TA is close to zero, although the  $S_1$  state of TQB-TA is a typical LE state. This should be induced by the strong symmetry of the molecule. Since TQB-TA is symmetric, the displacement vector  $r$  is nearly zero during excitation. Thus, the oscillator strength of TQB-TA is nearly zero.

### 3.5 Modification of TQB

Based on the results above, we found that only the single proton transfer is related to the light-emitting process. The second and third proton transfer are impossible to occur. In addition, we also found that the symmetric structure of TQB makes it non-radiative in  $S_1$ . Thus, we deduce that the molecule in the normal state can radiate if the symmetry is broken. Based on the above consideration, two molecules with only one hydrogen bond (TQB\*) or two hydrogen bonds (TQB\*\*) were designed (as shown in Fig. 8). It was found that the symmetry of the molecules is broken. The excited states and ESIPT states of the two molecules were investigated in toluene. Our calculation indicates that there is no ESIPT state for TQB\*, while only single proton transfer can occur for TQB\*\* (defined as TQB\*\*-TB). Consequently, only the proton transfer process of TQB\*\* was studied. The relaxed scanned potential energy curve of TQB\*\* is shown in Fig. 8(d). It can be found that TQB\*\*-TA (the normal state) is more stable than TQB\*\*-TB in  $S_0$ . The energy values for TQB\*\*-TA in  $S_1$  or  $T_1$  are quite close to that of TQB\*\*-TB. The energy barriers from TQB\*\*-TA to TQB\*\*-TB in both  $S_1$  and  $T_1$  (0.17 eV) are relatively higher than room temperature, which means that higher energy

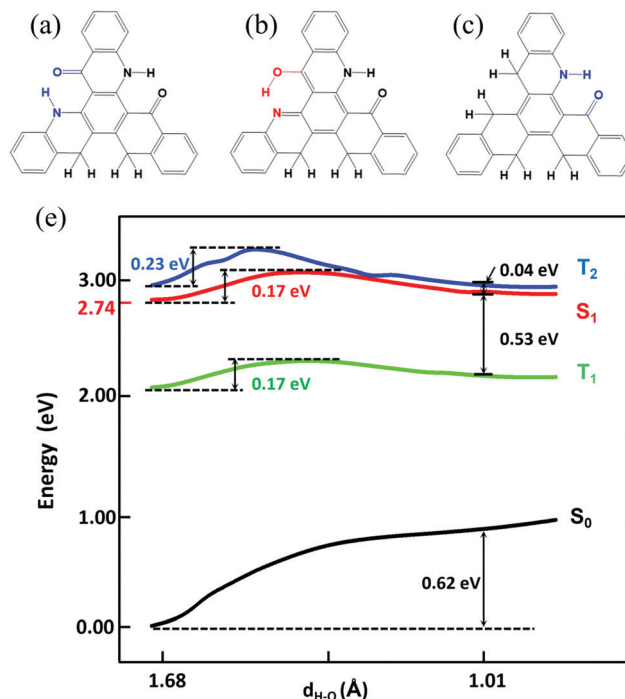


Fig. 8 Chemical structure of TQB\*\*-TA (a), TQB\*\*-TB (b), and TQB\*-TA (c). (d) Potential energy curve of TQB\*\* in toluene.

is needed for proton transfer. The energy barriers from TQB\*\*-TB back to TQB\*\*-TA are much lower in both  $S_1$  and  $T_1$ . This means that the forward and backward proton transfer processes can be controlled by external conditions. In addition, we also found that the energy of  $T_2$  is close to that of  $S_1$  during the proton transfer process, which may induce interaction between  $T_2$  and  $S_1$ . The energy levels of several low-lying excited states for TQB\*\*-TA and TQB\*\*-TB are illustrated in Fig. S5 (ESI<sup>†</sup>). It can be found that the energy gaps between  $S_1$  and  $T_1$  for TQB\*\*-TA and TQB\*\*-TB are 0.58 eV and 0.47 eV, respectively. The energy of  $T_2$  is close to that of  $S_1$ . In TQB\*\*-TA,  $T_2$  is 0.03 eV lower than  $S_1$ , while it is 0.07 eV higher than  $S_1$  in TQB\*\*-TB. The light-emitting properties were also studied for both TQB\*\*-TA and TQB\*\*-TB (as shown in Table 4). The emission wavelengths for TQB\*\*-TA and TQB\*\*-TB are 479 nm and 708 nm, respectively. It should be noted that the emission wavelengths (479 and 708 nm) here are the vertical emission wavelengths, which are different from the energy differences (2.74 and 2.6 eV) between  $S_1$  and  $S_0$ , respectively, in the optimized geometries, as shown Fig. S5 (ESI<sup>†</sup>). The oscillator strengths of TQB\* and TQB\*\* are 0.18 and 0.17, respectively, which are much larger than that of TQB-TA. The TDM of the two molecules are shown in Fig. S6 (ESI<sup>†</sup>). Significant TDM can be found,

Table 4 Emission wavelengths and oscillator strength calculated for TQB\*\* and TQB\* in toluene

	TQB**-TA	TQB**-TB	TQB*-TA
Wavelength (nm)	479	708	594
$f$	0.4702	0.1711	0.1839
$K_r$ ( $s^{-1}$ )	$1.53 \times 10^8$	$5.02 \times 10^7$	$4.48 \times 10^7$



which indicates that the molecule can radiate when the symmetry is broken. Based on the calculation results, we deduce that the TQB\*\* molecule can have dual emission and may be used as a light-emitting material for white light.<sup>35,36</sup> In addition, TADF may also be found since a large energy gap between  $T_2$  and  $T_1$  was found for both TQB\*\*TA and TQB\*\*TB, which means that the decay from  $T_2$  to  $T_1$  should be slow and favor the conversion from  $T_2$  to  $S_1$  due to their close energy levels. For TQB\*, the energy levels of several low-lying excited states are also shown in Fig. S5 (ESI†). We found that the energy gap between  $S_1$  and  $T_1$  is 0.38 eV, which is not favorable for upconversion. However, we found that the energy gap between  $T_2$  and  $T_1$  is as large as 0.99 eV, which means that the decay from  $T_2$  to  $T_1$  may be cut off. This is quite similar to the situation in the molecule with hybridized local and charge transfer (HLCT) excited states, as proposed by Ma' group.<sup>37–39</sup> In addition, the vertical excitation energy levels are shown in Fig. S7 (ESI†). It can be found that there is no excited state close in energy to  $T_2$ , and thus it is difficult for 'hot exciton' emission to occur. However, we also noticed that the energy gap between  $S_2$  and  $S_1$  is also much larger, which is a typical anti-Kasha's rule emission. Thus, we deduce that the TQB\* molecule may be used as a light-emitting molecule with anti-Kasha's rule emission.

## 4 Conclusions

In summary, the ESIPT and TADF mechanisms for TQB in both DMF and the solid state were studied based on the calculation of excited-state potential curves, energy levels and decay rates of the excited states. It was found that proton transfer in  $S_1$  for TQB is quite easy in both DMF and the solid phase. In contrast, the proton transfer in  $T_1$  or  $T_2$  in DMF is slightly difficult, while the barrier in  $T_1$  for TQB in the solid phase is comparable with room temperature energy. Thus, we concluded that proton transfer in the solid phase can be realized in both singlet and triplet excited states. For TQB, two TADF mechanisms were proposed: (1)  $T_2$ TQB-TB  $\rightarrow$   $S_1$ TQB-TB and (2)  $T_2$ TQB-TA  $\rightarrow$   $S_1$ TQB-TB. In DMF, the second mechanism should play a dominant role, while the first mechanism plays a significant role in the solid phase. In addition, the radiative property was found to be correlated with the symmetry and the proton transfer is accompanied by electron transfer. Finally, two molecules, TQB\* with a single hydrogen bond and TQB\*\* with two hydrogen bonds, were designed based on TQB. Based on our calculation results, we found that TQB\*\* can realize dual emission and be used in white light OLEDs. The energy gap between  $T_2$  and  $T_1$  as well as  $S_2$  and  $S_1$  for TQB\* is more than 1 eV, which may show anti-Kasha's rule emission. Our calculation results can not only help in understanding the light-emitting mechanism in the ESIPT-TADF molecule in both solution and the solid state, but also favor the design of functional luminescent molecules.

## Conflicts of interest

There are no conflicts to declare.

## Acknowledgements

This work is supported by the National Natural Science Foundation of China (Grant No. 11974216 and 11874242) and Shandong Provincial Natural Science Foundation, China (ZR2019MA056). Thanks to the supporting of Taishan Scholar Project of Shandong Province. Thanks to the supporting of the Project funded by China Postdoctoral Science Foundation (Grant No. 2018M642689).

## References

- 1 H. Uoyama, K. Goushi, K. Shizu, H. Nomura and C. Adachi, Highly efficient organic light-emitting diodes from delayed fluorescence, *Nature*, 2012, **492**(7428), 234–238.
- 2 J. Fan, Y. Zhang, K. Zhang, J. Liu, G. Jiang, L. Lin and C.-K. Wang, Effects of intramolecular and intermolecular interactions on excited state properties of two isomeric Cu complexes with AIE and TADF mechanisms in solid phase: A QM/MM study, *Org. Electron.*, 2019, **71**, 113–122.
- 3 J. Liu, Y. Zhang, K. Zhang, J. Fan, C.-K. Wang and L. Lin, Bicolor switching mechanism of multifunctional light-emitting molecular material in solid phase, *Org. Electron.*, 2019, **71**, 212–219.
- 4 T. Hatakeyama, K. Shiren, K. Nakajima, S. Nomura, S. Nakatsuka, K. Kinoshita, J. Ni, Y. Ono and T. Ikuta, Ultrapure Blue Thermally Activated Delayed Fluorescence Molecules: Efficient HOMO–LUMO Separation by the Multiple Resonance Effect, *Adv. Mater.*, 2016, **28**, 2777–2781.
- 5 H.-J. Park, S. H. Han and J. Y. Lee, A Directly Coupled Dual Emitting Core Based Molecular Design of Thermally Activated Delayed Fluorescent Emitters, *J. Mater. Chem. C*, 2017, **5**(46), 12143–12150.
- 6 X.-L. Chen, J.-H. Jia, R. Yu, J.-Z. Liao, M.-X. Yang and C.-Z. Lu, Combining Charge-Transfer Pathways to Achieve Unique Thermally Activated Delayed Fluorescence Emitters for High-Performance Solution-Processed, Non-doped Blue OLEDs, *Angew. Chem., Int. Ed.*, 2017, **56**(47), 15006–15009.
- 7 M. Mamada, K. Inada, T. Komino, W. J. Potscavage Jr., H. Nakanotani and C. Adachi, Highly Efficient Thermally Activated Delayed Fluorescence from an Excited-State Intramolecular Proton Transfer System, *ACS Cent. Sci.*, 2017, **3**(7), 769–777.
- 8 J. Zhao, S. Ji, Y. Chen, H. Guo and P. Yang, Excited state intramolecular proton transfer (ESIPT): from principal photophysics to the development of new chromophores and applications in fluorescent molecular probes and luminescent materials, *Phys. Chem. Chem. Phys.*, 2012, **14**, 8803–8817.
- 9 P. Zhou and K. Han, Unraveling the Detailed Mechanism of Excited-State Proton Transfer, *Acc. Chem. Res.*, 2018, **51**, 1681–1690.
- 10 J. E. Kwon and S. Y. Park, Advanced Organic Optoelectronic Materials: Harnessing Excited-State Intramolecular Proton Transfer (ESIPT) Process, *Adv. Mater.*, 2011, **23**, 3615–3642.
- 11 S. Park, O. H. Kwon, Y. S. Lee, D. J. Jang and S. Y. Park, Imidazole-Based Excited-State Intramolecular Proton-Transfer (ESIPT) Materials: Observation of Thermally Activated Delayed Fluorescence (TDF), *J. Phys. Chem. A*, 2007, **111**(39), 9649–9653.

- 12 J. Cao, J. Eng and T. J. Penfold, Excited State Intramolecular Proton Transfer Dynamics for Triplet Harvesting in Organic Molecules, *J. Phys. Chem. A*, 2019, **123**(13), 2640–2649.
- 13 J. Zhao, H. Dong, H. Yang and Y. Zheng, Solvent-Polarity-Dependent Excited-State Behavior and Thermally Active Delayed Fluorescence for Triquinolonobenzene, *ACS Appl. Bio. Mater.*, 2019, **2**, 2060–2068.
- 14 K. Wu, T. Zhang, Z. Wang, L. Wang, L. Zhan, S. Gong, C. Zhong, Z. H. Lu, S. Zhang and C. Yang, De Novo Design of Excited-State Intramolecular Proton Transfer Emitters via a Thermally Activated Delayed Fluorescence Channel, *J. Am. Chem. Soc.*, 2018, **140**, 8877–8886.
- 15 L. W. Chung, W. M. Sameera, R. Ramozzi, A. J. Page, M. Hatanaka, G. P. Petrova, T. V. Harris, X. Li, Z. Ke, F. Liu, H. B. Li, L. Ding and K. Morokuma, The ONIOM Method and Its Applications, *Chem. Rev.*, 2015, **115**(12), 5678–5796.
- 16 J. Fan, L. Cai, L. Lin and C. K. Wang, Dynamics of Excited States for Fluorescent Emitters with Hybridized Local and Charge-Transfer Excited State in Solid Phase: A QM/MM Study, *J. Phys. Chem. A*, 2016, **120**, 9422–9430.
- 17 J. Fan, L. Lin and C. K. Wang, Excited state properties of non-doped thermally activated delayed fluorescence emitters with aggregation-induced emission: a QM/MM study, *J. Mater. Chem. C*, 2017, **5**, 8390–8399.
- 18 L. Lin, J. Fan and C. K. Wang, Theoretical perspective for internal quantum efficiency of thermally activated delayed fluorescence emitter in solid phase: A QM/MM Study, *Org. Electron.*, 2017, **51**, 349–356.
- 19 M. J. Frisch; G. W. Trucks; H. B. Schlegel; G. E. Scuseria; M. A. Robb; J. R. Cheeseman; G. Scalmani; V. Barone; G. A. Petersson; H. Nakatsuji; X. Li; M. Caricato; A. V. Marenich; J. Bloino; B. G. Janesko; R. Gomperts; B. Mennucci; H. P. Hratchian; J. V. Ortiz; A. F. Izmaylov; J. L. Sonnenberg; D. Williams-Young; F. Ding; F. Lipparini; F. Egidi; J. Goings; B. Peng; A. Petrone; T. Henderson; D. Ranasinghe; V. G. Zakrzewski; J. Gao; N. Rega; G. Zheng; W. Liang; M. Hada; M. Ehara; K. Toyota; R. Fukuda; J. Hasegawa; M. Ishida; T. Nakajima; Y. Honda; O. Kitao; H. Nakai; T. Vreven; K. Throssell; J. A. Montgomery Jr.; J. E. Peralta; F. Ogliaro; M. J. Bearpark; J. J. Heyd; E. N. Brothers; K. N. Kudin; V. N. Staroverov; T. A. Keith; R. Kobayashi; J. Normand; K. Raghavachari; A. P. Rendell; J. C. Burant; S. S. Iyengar; J. Tomasi; M. Cossi; J. M. Millam; M. Klene; C. Adamo; R. Cammi; J. W. Ochterski; R. L. Martin; K. Morokuma; O. Farkas; J. B. Foresman and D. J. Fox, *Gaussian 16, Revision A.03*, Gaussian, Inc., Wallingford CT, 2016.
- 20 Z. Shuai and Q. Peng, Excited states structure and processes: Understanding organic light-emitting diodes at the molecular level, *Phys. Rep.*, 2014, **537**, 123–156.
- 21 Q. Peng, Y. Yi and Z. Shuai, Excited state radiationless decay process with Duschinsky rotation effect: Formalism and implementation, *J. Chem. Phys.*, 2007, **126**, 114302, DOI: 10.1063/1.2710274.
- 22 Y. Niu, Q. Peng and Z. Shuai, Promoting-mode free formalism for excited state radiationless decay process with Duschinsky rotation effect, *Sci. China, Ser. B: Chem.*, 2008, **51**, 1153–1158.
- 23 Y. Niu, Q. Peng, C. Deng, X. Gao and Z. Shuai, Theory of Excited State Decays and Optical Spectra: Application to Polyatomic Molecules, *J. Phys. Chem. A*, 2010, **114**, 7817–7831.
- 24 Q. Peng, Q. Shi, Y. Niu, Y. Yi, S. Sun, W. Li and Z. Shuai, Understanding the efficiency drooping of the deep blue organometallic phosphors: a computational study of radiative and non-radiative decay rates for triplets, *J. Mater. Chem. C*, 2016, **4**, 6829–6838.
- 25 H. Ma, W. Shi, J. Ren, W. Li, Q. Peng and Z. Shuai, Electrostatic Interaction-Induced Room-Temperature Phosphorescence in Pure Organic Molecules from QM/MM Calculations, *J. Phys. Chem. Lett.*, 2016, **7**, 2893–2898.
- 26 C. Lefebvre, G. Rubez, H. Khartabil, J. C. Boisson, C. G. Julia and E. Henon, Accurately extracting the signature of intermolecular interactions present in the NCI plot of the reduced density gradient versus electron density, *Phys. Chem. Chem. Phys.*, 2017, **19**, 17928–17936.
- 27 G.-J. Zhao, J.-Y. Liu, L.-C. Zhou and K.-L. Han, Site-Selective Photoinduced Electron Transfer from Alcoholic Solvents to the Chromophore Facilitated by Hydrogen Bonding: A New Fluorescence Quenching Mechanism, *J. Phys. Chem. B*, 2007, **111**, 8940–8945.
- 28 Dalton, A Molecular Electronic Structure Program, <http://daltonprogram.org>.
- 29 H. Sun, Z. Hu, C. Zhong, X. Chen, Z. Sun and J.-L. Bredas, Impact of Dielectric Constant on the Singlet-Triplet Gap in Thermally Activated Delayed Fluorescence Materials, *J. Phys. Chem. Lett.*, 2017, **8**(11), 2393–2398.
- 30 T. Lu and F. W. Chen, Multiwfn: A multifunctional wavefunction analyzer, *J. Comput. Chem.*, 2012, **33**, 580–592.
- 31 X. K. Chen, S. F. Zhang, J. X. Fan and A. M. Ren, Nature of Highly Efficient Thermally Activated Delayed Fluorescence in Organic Light-Emitting Diode Emitters: Nonadiabatic Effect between Excited States, *J. Phys. Chem. C*, 2015, **119**, 9728–9733.
- 32 J. Gibson, A. P. Monkman and T. J. Penfold, The Importance of Vibronic Coupling for Efficient Reverse Intersystem Crossing in Thermally Activated Delayed Fluorescence Molecules, *Chem. Phys. Chem.*, 2016, **17**, 2956–2961.
- 33 C. M. Marian, Mechanism of the Triplet-to-Singlet Upconversion in the Assistant Dopant ACRXTN, *J. Phys. Chem. C*, 2016, **120**, 3715–3721.
- 34 P. K. Samanta, D. Kim, V. Coropceanu and J. L. Brédas, Up-Conversion Intersystem Crossing Rates in Organic Emitters for Thermally Activated Delayed Fluorescence: Impact of the Nature of Singlet vs Triplet Excited States, *J. Am. Chem. Soc.*, 2017, **139**, 4042–4051.
- 35 B. Li, L. Zhou, H. Cheng, Q. Huang, J. Lan, L. Zhou and J. You, Dual-emissive 2-(2'-hydroxyphenyl) oxazoles for high performance organic electroluminescent devices: discovery of a new equilibrium of excited state intramolecular proton transfer with a reverse intersystem crossing process, *Chem. Sci.*, 2018, **9**, 1213–1220.
- 36 L. Duarte, J. Germino, J. Berbigier, C. Barboza, M. Faleiros, D. Simoni, M. Galante, M. Holanda, F. Rodembusch and T. Atvars, White-light generation from all-solution-processed

- OLEDs using a benzothiazole-salophen derivative reactive to the ESIPT process, *Phys. Chem. Chem. Phys.*, 2019, **21**, 1172–1182.
- 37 L. Yao, B. Yang and Y. Ma, Progress in next-generation organic electroluminescent materials: material design beyond exciton statistics, *Sci. China: Chem.*, 2014, **57**, 335–345.
- 38 X. Tang, Q. Bai, Q. Peng, Y. Gao, J. Li, Y. Liu, L. Yao, P. Lu, B. Yang and Y. Ma, Efficient Deep Blue Electroluminescence with an External Quantum Efficiency of 6.8% and CIEy < 0.08 based on a Phenanthroimidazole-Sulfone Hybrid Donor-Acceptor Molecule, *Chem. Mater.*, 2015, **27**, 7050–7057.
- 39 D. Hu, L. Yao, B. Yang and Y. Ma, Reverse intersystem crossing from upper triplet levels to excited singlet: a ‘hot excitation’ path for organic light-emitting diodes, *Philos. Trans. R. Soc., A*, 2015, **373**, 20140318.